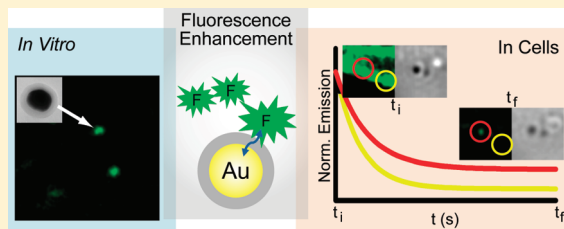


Detection of Low Quantum Yield Fluorophores and Improved Imaging Times Using Metallic Nanoparticles

Laura C. Estrada,^{†,||} M. Julia Roberti,[‡] Sabrina Simoncelli,[‡] Valeria Levi,[§] Pedro F. Aramendía,^{*,‡} and Oscar E. Martínez[†]

[†]Departamento de Física, [‡]INQUIMAE-Departamento de Química Inorgánica, Analítica y Química Física, and [§]Departamento de Química Biológica, Facultad de Ciencias Exactas y Naturales, Universidad de Buenos Aires, 1428 Buenos Aires, Argentina

ABSTRACT: The behavior of a fluorophore near a gold nanoparticle is rationalized by a theoretical description of the parameters that modify the fluorescence emission: nanoparticle–fluorophore distance, fluorescence quantum yield (ϕ^0), and fluorophore absorption and emission spectra, to find optimum conditions for designing fluorophore–nanoparticle probes. The theoretical maximum gain in brightness of the nanoparticle–fluorophore system with respect to the isolated molecule increases almost inversely proportional to ϕ^0 . The brightness enhancement in imaging experiments *in vitro* was assessed by using Au–SiO₂ core–shell nanoparticles deposited on glass. A ~ 13 -fold emission brightness enhancement for weakly fluorescent molecules was observed. A significant increase in fluorophore photostability, rendering longer imaging times, was obtained for fluorophores interacting with gold nanoparticles incorporated by endocytosis in cells. Our results illustrate a way to increase imaging times and to study molecules in the vicinity of a metallic nanoparticle after photobleaching of background fluorescence.



INTRODUCTION

The interaction of chromophores with metallic nanoparticles (NPs) has been extensively studied in recent years.¹ Fluorophores (Fs) in close vicinity to such NPs are interesting systems to develop sensors, especially in the fields of cellular tracking and imaging. Fluorescence enhancement of a fluorophore at distances in the nanometer scale from a metallic NP is well documented,² a phenomenon attributed to the near-field interaction of the molecule oscillating transition dipole with a characteristic resonance frequency of the free electrons of the nanostructure. Because of this interaction, metallic NPs can modify the emission of fluorescent molecules by increasing the excitation and emission rates (plasmonic enhancement), as well as by modifying the nonradiative energy transfer from the molecule to the particle (quenching effect). These processes are influenced by the NP size, shape, and material, the fluorophore absorption and emission properties, quantum yield (ϕ^0), orientation; NP–F distance (h); and the dielectric constant of the surrounding medium.³ The distance-dependent changes in excitation, emission, and nonradiative energy transfer rates yield an overall fluorescence quenching at very short distances from the NP, while emission enhancement is observed at intermediate distances, and no influence results for a molecule placed at a distance greater than about twice the NP radius (a). Therefore, it becomes clear that a careful analysis of the characteristics of the NP–F system on the fluorescence emission is of broad interest to find conditions that optimize desirable properties of the probe, namely, its brightness and photostability.

The increment of the radiative and nonradiative decay rates of the fluorophore has been confirmed by the decrease in

fluorescence lifetime and enhancement of fluorescence intensity. Previous reports of fluorescence enhancement of fluorophores by silver island films bound to metallic nanostructures⁴ addressed in a quantitative manner some particular aspects on how the distance between the metal and the molecule modifies the emission intensity, the extent of the enhanced region, and the role of the photophysical properties of the fluorophore (fluorescence quantum yield ϕ^0 and excitation and fluorescence emission spectra). A comprehensive characterization of these parameters can be exploited to engineer NP–F systems with tailored properties, of interest in fluorescence-based spectroscopies and imaging techniques. The challenges here are to improve single molecule fluorescence detection and to provide higher stability against photobleaching. Thus, the need of a global analysis of all the variables to be taken into account when analyzing the fluorescence enhancement phenomenon becomes clear.

We have previously demonstrated in fluorescence correlation spectroscopy (FCS) experiments on gold nanoparticles (AuNPs) that the volume of observation can be drastically reduced below the diffraction limit, with a simultaneous increase in the detectable fluorophore concentration range.⁵ Here, we provide a thorough description of the interplay between the parameters that contribute to the fluorescence enhancement, which are relevant for the rational design of NP–F systems. Our analysis provides specific guidelines to establish the optimum NP–F

Received: September 30, 2011

Revised: December 28, 2011

Published: January 11, 2012

distance (h) that maximizes the gain in molecular brightness and the total number of emitted photons before photobleaching. Also, we include the effect of quantum yield to determine the optimum ϕ^0 of the isolated fluorophore to achieve the better contrast between the NP-influenced fluorophore and the background.

Fluorescence enhancement is represented by two parameters of practical significance. The first is the gain in brightness (GB), defined as the increase in the rate of fluorescence emission of the molecule interacting with the metallic NP, relative to an isolated one. The second is the gain in total emitted photons (GP), defined as the average total number of photons emitted by a molecule before photobleaching when interacting with a metallic NP, also relative to an isolated molecule. We present the theoretical expressions for GB and GP for fluorescent molecules interacting with spherical AuNPs of radius in the range of 5–40 nm. We analyze the dependence of GB and GP on h , ϕ^0 , and fluorophore absorption and emission maximum wavelengths. The calculations indicate that fluorescence enhancement is significantly higher for fluorophores with low ϕ^0 . Fluorescence imaging of AuNPs and the chromophore Rose Bengal in vitro provide evidence for the detection of low quantum yield molecules via emission enhancement by AuNPs, and experiments in cells show the feasibility of extending imaging times of a fluorophore.

EXPERIMENTAL METHODS

Chemicals. All reagents were of analytical grade (Sigma, USA). Cell culture media were from Sigma and Invitrogen (USA).

Nanoparticle Preparation. AuNPs with an average radius of $a = 30 \pm 3$ nm (sample set size $n > 10$) were prepared in our lab by reduction of an aqueous Au(III) solution using mercaptosuccinic acid, as described in the literature.⁶ The final NP concentration was ~ 1 nM. The mean radius was measured by transmission electron microscopy (TEM) in a Philips EM 301 apparatus.

Au–SiO₂ core–shell nanoparticles (Au–SiO₂-NPs) were synthesized as described elsewhere.⁷ The AuNPs employed for the core were synthesized as cited above. We obtained three batches with different final SiO₂ shell thicknesses: 8 ± 2 nm, 18 ± 2 nm, and 40 ± 2 nm, estimated from TEM images (sample set size $n > 10$ in all cases).

SiO₂ nanoparticles employed as control samples were prepared using a standard Stöber protocol.⁸ The mean radius, from TEM measurements, was 60 ± 4 nm (sample set size $n > 10$).

In all cases, image processing was performed with ImageJ (NIH, USA) and DIPImage (TU-Delft, Netherlands) toolbox for MATLAB (The MathWorks, Natick, USA).

In Vitro Experiments. Fluorescence enhancement was tested with Au–SiO₂-NPs deposited on glass coverslips and immersed in a 1 μ M dye solution. The net negative charge on the NP surface required a positively charged surface to attach them via electrostatic forces. Therefore, we treated the glass coverslips as follows. First, they were cleaned with NaOH 1 M at 60 °C for 1 h and then rinsed thoroughly with water. The surface was functionalized with aminopropyltriethoxysilane (APTES) by using the following protocol: the coverslips were immersed in a 2% v/v aqueous APTES solution, let stand for 1 h, washed 3 times in an ultrasound bath with acetone, and then dried at room temperature. Nanoparticle deposition was carried out by adding a drop of the corresponding stock solution on the coverslip (AuNPs, with or without the SiO₂ shell, or SiO₂ control sample), rinsing after 15 min with water and then left to

dry at room temperature. The fluorophore solution was prepared by dissolving either Rose Bengal or Rhodamine B in Milli-Q water, to a 1 μ M concentration. A drop of the fluorophore solution was placed onto the coverslip containing the NPs and imaged. Fluorescence imaging was carried out in an Olympus FV1000 confocal microscope (Olympus, Japan), using a 543 nm He–Ne laser for sample excitation and a 60 \times , 1.35 NA oil immersion objective. Fluorescence emission was observed in the spectral detection channel (bandwidth 570–670 nm).

Simultaneously, transmission images were acquired in a separate channel of the microscope, in order to localize and identify the NPs. With this purpose, the plasmon absorption was tested by sequentially irradiating the samples with the available laser excitation lines (458, 488, 515, 543, and 635 nm) and detecting the outcoming signal in the transmission channel of the microscope.

Digital image analysis was performed with the software mentioned above.

Cell Measurements. *Xenopus laevis* melanophores were cultured as previously described⁹ in the presence of phenylthiourea (PTU) to inhibit melanin biosynthesis. Upon reaching 90% confluence, the cells were split and plated onto 12 mm nontreated glass coverslips, using L-15 medium supplemented with 4% FBS and antibiotics (complete medium).

For endocytosis experiments, culture medium was removed and replaced by PBS buffer. The cells were starved for two hours and then returned to complete medium containing a 1:10 dilution of a stock solution of the synthesized AuNPs without any SiO₂ coating and incubated overnight at 27 °C. Control samples without AuNPs were also prepared. Actin staining was performed 12 h after AuNPs addition, using Texas Red X phalloidin (TRedX-phal, Invitrogen, USA) as follows. Cells were fixed with PFA 4% for 15 min on ice, washed three times with TBS buffer, and then permeabilized with PBS + 0.01% Triton X100. To reduce nonspecific binding, cells were incubated for 5 min with PBS + 1% BSA. A methanol stock solution of TRedX-phal was prepared according to the manufacturer's indication (Invitrogen). The cells were then incubated with a 1:200 TRedX-phal dilution in PBS for 15 min and afterward washed three times with PBS. The coverslips were mounted in PBS for their observation.

Fluorescence imaging was performed in the Olympus FV1000 confocal microscope described above. Cells were observed using a 543 nm He–Ne laser for excitation. For the photobleaching experiments, the laser was set to maximum output power (~ 200 μ W), and a time sequence of images was acquired. Emission was detected with the spectral detection channel (bandwidth 555–650 nm). A 565 nm long-pass filter was placed before the detector to filter out scattered laser light. The associated pre- and postbleaching emission spectra were acquired with the same spectral channel, using a bandwidth of 10 nm and a scanning step of 5 nm between 555 and 650 nm.

Image processing was performed as previously described.

RESULTS AND DISCUSSION

Theoretical Background. It is known¹⁰ that the interaction of a metallic NP with a fluorophore affects the rates of excitation (γ_{exc}) and radiative emission (γ_{rad}). This interaction introduces at the same time a dissipative electronic energy transfer pathway from the excited fluorophore to the NP (γ_{abs}) that is absent in the isolated fluorophore. We will assume for our calculations that other nonradiative rate constants of the isolated molecule, such as the photobleaching (γ_{pb}) and the

internal conversion (γ_{nr}), are not affected by the presence of the NP. In what follows, variables with a zero superscript correspond to the isolated molecule, and those without superscript, to the NP–F system. We will analyze the photophysical performance of a fluorophore as a function of the NP–F distance (h), the intrinsic emission quantum yield of the molecule (ϕ^0), its absorption and emission maximum, and NP radius (a).

The fluorescence quantum yield is expressed by

$$\phi = \frac{\gamma_{\text{rad}}}{\gamma_{\text{rad}} + \gamma_{\text{nr}} + \gamma_{\text{pb}} + \gamma_{\text{abs}}} \quad (1)$$

which can be rewritten as

$$\phi = \frac{\gamma_{\text{rad}}/\gamma_{\text{rad}}^0}{\gamma_{\text{rad}}/\gamma_{\text{rad}}^0 + \gamma_{\text{abs}}/\gamma_{\text{rad}}^0 + \frac{1-\phi^0}{\phi^0}} \quad (2)$$

The gain in brightness, GB, depends on the emission quantum yield and on the excitation rate ratios, as expressed by

$$\text{GB} = \frac{\gamma_{\text{exc}}}{\gamma_{\text{exc}}^0} \frac{\phi}{\phi^0} \quad (3)$$

Importantly, eq 3 shows that a high GB can be obtained either by an excitation rate enhancement or by increasing the relative quantum yield of emission.

The increase in the total number of emitted photons depends only on the radiative rate constant increase, as given by¹¹

$$\text{GP} = \frac{\gamma_{\text{rad}}}{\gamma_{\text{rad}}^0} \quad (4)$$

The relationship between γ_{exc} , γ_{rad} , and γ_{abs} with NP geometry, the transition dipole of F, the absorption and emission frequency, and the dielectric constant of the medium, can be obtained using rigorous multipole methods.¹² However, it has been shown that classical electrodynamics agrees surprisingly well with more rigorous calculations.^{12b} For this reason, we use that simplified analytical model to describe the emission properties of F in the proximity of a metallic NP. Nevertheless, one has to keep in mind that even if classical electrodynamics agrees well with experimental results for nanospheres, these results should not be extended to other geometries of nanoparticles often met in plasmonics.^{4b}

When F is placed in the proximity of a metallic NP at a distance h , an electric field resulting from the presence of the NP, E_s , is added to the excitation electric field, $E_0(h, \omega_{\text{exc}})$. Therefore, the total field acting at the molecule location on its transition dipole moment, μ , is $E_0(h, \omega_{\text{exc}}) + E_s(h, \omega_{\text{exc}})$. Assuming a spherical particle of radius a , small compared to the wavelength of excitation, and F with its transition dipole aligned in the light polarization direction (when the transition dipole moment is oriented at an angle θ relative to the polarization direction of the incident electric field, the excitation rate increase in eq 5 is multiplied by $\cos^2\theta$), the excitation enhancement can be expressed as

$$\frac{\gamma_{\text{exc}}}{\gamma_{\text{exc}}^0} = \left| 1 + 2 \frac{1}{\left(1 + \frac{h}{a}\right)^3} \frac{\varepsilon(\omega_{\text{exc}}) - \varepsilon_{\text{m}}}{\varepsilon(\omega_{\text{exc}}) + 2\varepsilon_{\text{m}}} \right|^2 \quad (5)$$

where $\varepsilon(\omega_{\text{exc}})$ is the frequency-dependent dielectric constant of gold at the excitation frequency, and ε_{m} , the dielectric constant of

the surrounding medium. In this work, we consider only NPs with $a > 10$ nm to avoid size effects in the NP dielectric constant.¹³

According to eq 3, a complete analysis of GB requires the consideration of all the conditions that affect ϕ . For very small NP–F distances ($h \ll a$), the quenching effect of the NP can be approximated by that of a planar surface. Using electrostatic image theory,^{12b} the electronic energy transfer rate from the excited molecule to the metallic NP can be calculated. The effectiveness of this nonradiative decay via energy transfer decreases with h . This decay rate, γ_{abs} , when normalized to γ_{rad}^0 , can be expressed as a dissipative term (D),

$$D = \frac{\gamma_{\text{abs}}}{\gamma_{\text{rad}}^0} = \frac{3}{16} \text{Im} \frac{\varepsilon(\omega_{\text{em}}) - \varepsilon_{\text{m}}}{\varepsilon(\omega_{\text{em}}) + \varepsilon_{\text{m}}} \frac{1}{k_{\text{em}}^3 h^3} \frac{(\mu_x^2 + \mu_y^2 + 2\mu_z^2)}{|\mu|^2} \quad (6)$$

where the z coordinate is defined as the direction in which the incident field is polarized, $\varepsilon(\omega_{\text{em}})$ is the dielectric constant of gold at the maximum emission frequency of F, and k_{em} is the wave vector modulus in the surrounding medium at ω_{em} . Notice the rapid decrease of this term with the distance as $1/h^3$, and its divergence at $h = 0$, which supports the planar interface approximation.

Finally, the derivation of the relative radiative decay rate considers the fact that, in the presence of the metallic NP, the dipole moment of the molecule changes from μ to $\mu + \mu_{\text{induced}}$. Then, for F with a transition dipole aligned in the polarization direction, the decay rate, γ_{abs} , when normalized to γ_{rad}^0 , is

$$\frac{\gamma_{\text{rad}}}{\gamma_{\text{rad}}^0} = \left| 1 + 2 \frac{1}{\left(1 + \frac{h}{a}\right)^3} \frac{\varepsilon(\omega_{\text{em}}) - \varepsilon_{\text{m}}}{\varepsilon(\omega_{\text{em}}) + 2\varepsilon_{\text{m}}} \right|^2 \quad (7)$$

The expressions given in eqs 5 and 7 for the excitation enhancement and the relative radiative decay rate are identical. This fact has been pointed out previously,¹⁴ but it does not hold for all molecular orientations relative to the incident electric field. For example, if the transition dipole moment of F is aligned perpendicular to the light polarization direction, the relative radiative decay rate is

$$\frac{\gamma_{\text{rad}}}{\gamma_{\text{rad}}^0} = \left| 1 - \frac{1}{\left(1 + \frac{h}{a}\right)^3} \frac{\varepsilon(\omega_{\text{em}}) - \varepsilon_{\text{m}}}{\varepsilon(\omega_{\text{em}}) + 2\varepsilon_{\text{m}}} \right|^2 \quad (8)$$

which differs from eq 5.

It is noteworthy to point out that the excitation enhancement has its maximum at $h = 0$ (eq 5), but the normalized dissipative decay rate increases infinitely fast at $h = 0$ (eq 6). As a result, there is a region of very low brightness near the NP surface, whose extension depends on a and ϕ^0 . Farther away, and as a result of these two competitive effects, either fluorescence quenching or fluorescence enhancement can be observed by changing h .

GB and GP in NP–F Systems. In this section, we present the results of the calculations of GB and GP as a function of

ϕ^0 , h , a , and the absorption and emission maxima of F. To compute GB, which depends both on the excitation and emission frequencies (eqs 2, 3, and 5–7), we assume that F has a Stokes shift of 30 nm, which is in the order of those typically observed for standard dyes. Also, we restrict our analysis to AuNPs. In view of the potential biological applications of NP–F systems, AuNPs fulfill the conditions of providing a significant enhancement and being chemically inert and biocompatible at the same time.

First, we calculate the relative increase in NP–F emission quantum yield, ϕ/ϕ^0 , as a function of h for AuNP with $a = 30$ nm in water, and excited at the plasmon maximum, $\lambda_{\text{exc}} = 540$ nm (Figure 1A). We use the Au dielectric constant from the

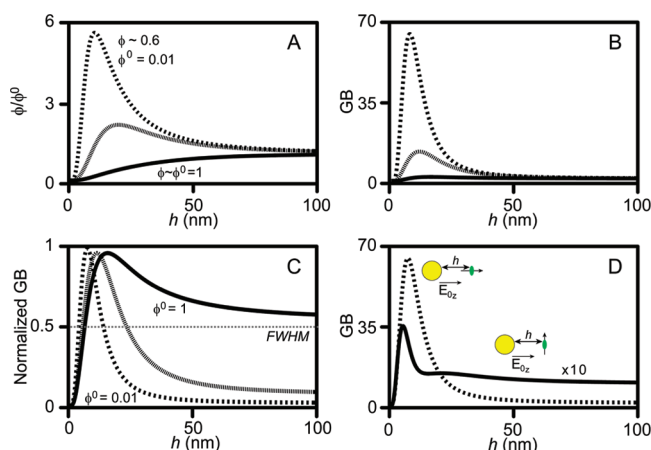


Figure 1. (A) Calculated relative emission quantum yield for a 30 nm radius AuNP–F in water, for a molecule excited at $\lambda_{\text{exc}} = 540$ nm and emitting at 570 nm as a function of the NP–fluorophore distance, h , for the case of light polarization direction parallel to the absorption and emission transition dipoles. (—, $\phi^0 = 1$; ---, $\phi^0 = 0.1$; - - -, $\phi^0 = 0.01$). (B) Corresponding GB curves. (C) Corresponding maximum normalized GB, showing the decrease in the fwhm as ϕ^0 diminishes. (D) GB estimation for a molecule whose transition dipole is oriented either parallel (—) or perpendicular (---, displayed values are multiplied by 10) to the incident light polarization direction.

literature¹⁵ and assume that the transition dipole of the molecule is aligned in the direction of the polarization of the incident light beam. As expected, no increase in the NP–F quantum yield is observed for $\phi^0 = 1$, whereas the maximum in ϕ/ϕ^0 , rapidly increases with decreasing ϕ^0 . The dependence of GB with h (Figure 1B) shows two distinct behaviors; a strong quenching is observed at very small h values, attributed to the prevalence of the nonradiative pathway that transfers electronic energy from the molecule to the NP.^{2e,10,16} The results indicate that when $\phi^0 = 1$, $\text{GB} < 0.1$ for $h < 1.8$ nm, while for $\phi^0 = 0.1$ and 0.01, that region is restricted to $h < 0.75$ and 0.35 nm, respectively. Larger values of h define a region of sharp increase in ϕ between 5 and 10 nm. Considering that GB depends on the product of the excitation rate and ϕ^0 ratios (eq 3) and the fact that the plot of ϕ/ϕ^0 shows no maximum with distance for $\phi^0 = 1$, we can conclude that the increase in GB for $\phi^0 = 1$ arises in the excitation rate increase. For lower values of ϕ^0 , the increase in GB shows contributions from the excitation rate enhancement as well as from the increase on the relative ϕ . Also, the maximum GB increases with decreasing ϕ^0 (Figure 1B), whereas the position of this maximum approaches the surface of the NP as ϕ^0 decreases (Figure 1C). The region of enhancement, quantified by the full width at half-maximum

(fwhm) of the GB curves as a function of h , strongly depends on ϕ^0 , becoming narrower as ϕ^0 decreases. For $\phi^0 = 0.1$, fwhm ~ 20 nm, whereas for $\phi^0 = 0.01$, fwhm ≈ 10 nm. These results show that the value of ϕ^0 plays a key role in defining the enhanced region and imply that a significant reduction in the volume where brightness enhancement takes place can be obtained using weakly fluorescent molecules.⁵ This feature is more evident upon examination of the normalized curves (Figure 1C). Finally, Figure 1D shows the GB dependence on h for two extreme orientations of the dipole moment of the fluorophore with respect to the polarization of the incident light. As expected, the perpendicular orientation leads to a much weaker GB than the parallel one. These two extreme cases must be kept in mind when considering actual GB values in randomly oriented fluorophore samples.

The relationship between the maximum value for GB and h as a function of ϕ^0 can be advantageously employed in the design of NP–F hybrid probes (Figure 2). The maximum GB

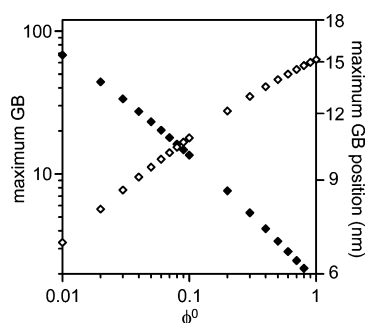


Figure 2. Maximum calculated gain in brightness, GB (\blacklozenge) and its position from de NP surface (\diamond) for a 30 nm radius AuNP–F system in water, as a function of the intrinsic molecule quantum yield, ϕ^0 ($\lambda_{\text{exc}} = 540$ nm; $\lambda_{\text{em}} = 570$ nm). Values are given for a fluorescent molecule with the transition and absorption moments parallel and aligned with the light polarization direction.

increases almost inversely proportional to ϕ^0 and indicates, for each fluorophore, the most appropriate distance to place it from the NP surface. Even though the maximum value for GB increases as ϕ^0 decreases, the product between the maximum GB and ϕ^0 steadily decreases with ϕ^0 , thus preventing to achieve higher absolute brightness with less fluorescent molecules.

The maximum GB value and its position from the NP surface can also be calculated as a function of a for $\phi^0 = 0.1$ and 0.01 (Figure 3). The dependence with a arises because the excitation enhancement scales with the ratio h/a (eq 5), while D (the dissipation to the AuNP), scales with the distance h (eq 6). The results suggest that variations in NP size within 10%, which is the expected size dispersion in NP batches, do not translate into large variations in the position of the maximum GB from the NP surface. In contrast, the value of the maximum GB shows a monotonous growth with the increase in the NP radius. For molecules with $\phi^0 = 0.01$, a 2-fold change in a produces a 4-fold change in the value of the maximum GB (Figure 3B). Finally, it is important to notice that as ϕ^0 increases, it is necessary to use larger NPs to obtain a gain in brightness ($\text{GB} > 1$). If we consider a $\text{GB} > 5$ as an indication of an overall enhancement (taking into account that the curves shown were calculated for parallel transition dipole and incident light polarization), this condition is fulfilled for NP of $a > 20$ nm for fluorophores with $\phi^0 = 0.1$ (Figure 3A) and for NP of $a > 10$ nm for molecules with $\phi^0 = 0.01$ (Figure 3B). For highly

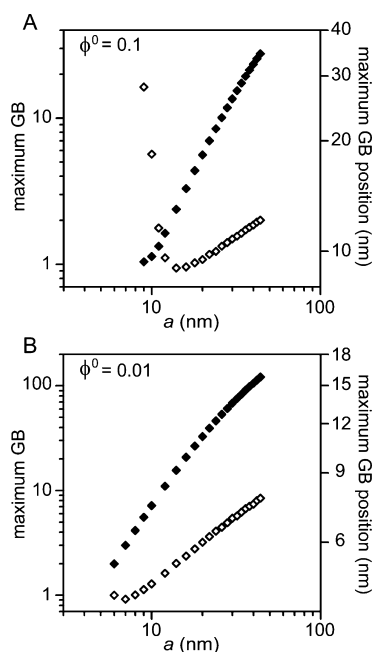


Figure 3. Maximum calculated gain in brightness, GB, (\blacklozenge) and its position from the NP surface (\diamond) for a 30 nm radius AuNPFH system in water as a function of the NP radius, a . Values are given for a fluorescent molecule with the transition and absorption moments parallel and aligned with the light polarization direction ($\lambda_{\text{exc}} = 540$ nm; $\lambda_{\text{em}} = 570$ nm). (A) $\phi^0 = 0.1$; (B) $\phi^0 = 0.01$.

fluorescent molecules ($\phi^0 \approx 1$), GB > 1 is obtained for AuNPs of $a > 35$ nm.

The other parameter representing the emission enhancement is GP (eq 4). GP depends only on γ_{rad} and γ_{rad}^0 , and as expressed by eqs 7 and 8, it decreases monotonically with h . The dependence of GB and GP with the maximum emission wavelength of F reveals further interesting aspects relevant to the design parameters of NP–F systems. It is useful to compare the dependence of GB, of the dissipative term D (eq 6), and of GP, with the maximum emission wavelength of F (we maintain the assumption of a ~ 30 nm Stokes shift for F), for a weak fluorescent molecule ($\phi^0 = 0.01$) aligned in the polarization direction (Figure 4). We focus our analysis on weakly fluorescent molecules for the greater values in GB and GP obtained with them, as opposed to fluorophores with higher ϕ^0 . When F is placed at $h = 1$ nm from a AuNP of $a = 30$ nm, the dissipation to the NP dominates the photophysics of the system. Thus, the maximum values of GB and GP are observed for fluorophores of very different emission wavelength (Figure 4A). The maximum GB is obtained for molecules emitting near 650 nm, whereas the maximum for GP occurs when emission is near 525 nm. As a result, at very small distances to the NP, the molecule absorption and emission wavelengths can be chosen to optimize either GB or GP separately, which in principle provides a selectivity tool for the design of a NP–F probe. For example, a 30-fold enhancement in GP (or in observation time under equal brightness) is reached for molecules emitting near 525 nm, at the expense of achieving only GB ≈ 2 under these conditions. At a short distance from the NP, the dissipative term limits the excited state lifetime and provides the prolonged photostability. This is at the expense of brightness but in adequate conditions can be advantageous. The situation changes significantly upon increasing h because the dissipative term rapidly decreases. At $h = 10$ nm, both γ_{rad} and γ_{abs} become

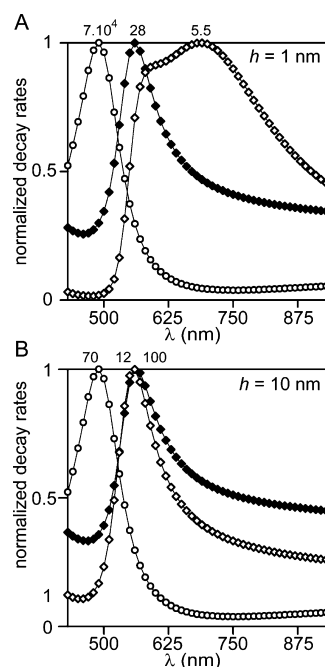


Figure 4. Calculated gain in photons, GP, (\blacklozenge), gain in brightness, GB, (\diamond), and relative dissipative decay rate, D , (\circ), for a weakly fluorescent molecule ($\phi^0 = 0.01$) in water as a function of the maximum emission wavelength of the dye. GB estimated for a molecule with a Stokes shift of 30 nm. Plots are shown normalized to the respective maximum, whose value is shown in the figure accompanying the corresponding curve. Curves are calculated for a fluorescent molecule in the vicinity of a 30 nm AuNP with the transition and absorption moments parallel and aligned in the light polarization direction. (A) At $h = 1$ nm from the NP surface; (B) at $h = 10$ nm from the NP surface.

similar and consequently the wavelength dependence of GP and GB is almost the same with a maximum GB for F emitting near 550 nm and a maximum GP for F emitting near 530 nm (Figure 4B). Even though the emission wavelength at which GB and GP have a maximum value are not the same, the value for GP is at 85% of its maximum at the wavelength of maximum GB (and vice versa). Under these conditions, it is possible to simultaneously enhance GP and GB values by choosing F with an emission in the 530–550 nm interval and when placed at $h = 10$ nm.

In Vitro Detection of Low Quantum Yield Fluorophores. To test the previous calculations, we first carried out experiments on AuNPs fixed on a glass surface immersed in 1 μM solutions in water of dyes with similar spectral properties and very different ϕ^0 . In particular, we used (Figure 5A) Rose Bengal ($\phi^0 = 0.02$)¹⁷ and RhodamineB ($\phi^0 = 0.31$).¹⁸ To set h , we synthesized core–shell AuNP–SiO₂ nanoparticles (Figure 5B), so that the dye in solution would not be accessible to the Au surface beyond the limit imposed by the SiO₂ shell during imaging. Additionally, the possible adsorption effects arising from the SiO₂ coating were accounted for by testing a control sample of NPs composed of SiO₂ only, i.e., without the Au core (Figure 5B).

Image acquisition was performed using two-channel detection, one to detect the fluorescence intensity signal and another to record the transmitted light (Figure 5C). An inspection of the transmission images of the samples acquired at the confocal microscope shows distinctive structures on the glass that in principle correspond to AuNPs (Figure 5C). To positively identify these structures as AuNPs, we took advantage of the

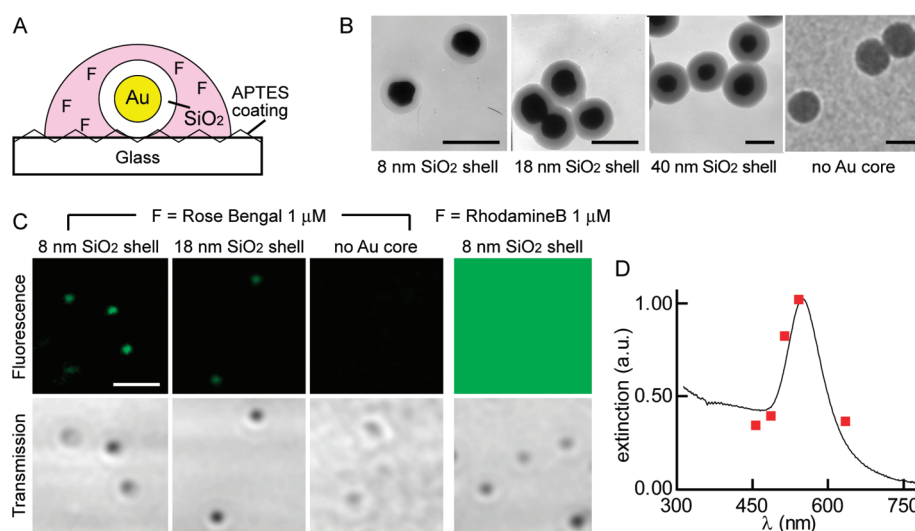


Figure 5. (A) Schematics of sample preparation for the confocal microscopy experiments in vitro: Au–SiO₂ core–shell nanoparticles were deposited on APTES-derivatized glass coverslips, then covered with a solution of the fluorophore of interest (F = Rose Bengal or Rhodamine B). (B) TEM micrographs of the Au–SiO₂ core–shell nanoparticles with increasing SiO₂ shell thickness, and control sample with SiO₂ nanoparticles (without Au core). Scale bars: 100 nm in all cases. (C) Confocal fluorescence intensity (top) and transmission (bottom) images recorded by raster-scanning Au–SiO₂ core–shell nanoparticles in the presence of either 1 μ M Rose Bengal or Rhodamine B aqueous solutions. The nanoparticle samples correspond to 8 and 18 nm thick SiO₂ shells, and a control sample of 60 nm radius pure SiO₂ NPs is also shown. Scale bar: 1 μ m. (D) Normalized extinction values for single AuNPs using the five available laser excitation wavelengths (458, 488, 515, 543, and 635 nm) (red points) and extinction spectrum of a suspension of AuNP acquired at a spectrophotometer (solid line).

fact that the plasmon absorption of metallic NPs is strongly dependent on the size, shape, and NP material, and performed a spectral characterization of the transmitted signal. To this end, we measured the transmission images that correspond to the different laser excitation wavelengths available in the microscope. For each spot regarded as a NP, we calculated the corresponding background-corrected intensity value (Figure 5D), obtained the normalized extinction values at the given wavelengths, and superimposed the values with the extinction spectrum of a suspension of AuNPs. The data taken in the suspension and on individual spots of the transmission image agree very well, thus confirming that the spotted structures in the transmission images are indeed AuNPs.¹⁹ As a simplified method, the extinction ratio T at 488 and 543 nm for the AuNPs, $T_{488}/T_{543} \approx 0.5$, served as criterion to positively identify and single them out from structures that only scatter light (in which case $T_{488}/T_{543} > 1$). This procedure can be applied to denuded AuNPs and core–shell AuNP–SiO₂ as well since SiO₂ does not significantly interfere with the plasmon absorption.

Once the NPs were located, the associated fluorescence images were acquired (Figure 5C). Upon addition of the Rose Bengal solution, a clear fluorescence signal against background was observed for silica shells of 8 and 18 nm, whereas no significant intensity was distinguishable for the thick shells of 40 nm (image not shown) and with SiO₂ control nanoparticles. The absence of signal for the SiO₂ nanoparticles indicates that there is no significant contribution of eventually adsorbed dye on the surface that could be responsible for the increase in fluorescence. Importantly, the absence of signal at high values of h confirms that for such long distances, the dye is not capable of interacting with the AuNP, and thus, the enhancement effect is negligible.

For each mean thickness of the SiO₂ shell, the average intensity associated to each NP in the images was calculated by masking the structures and measuring the mean fluorescence

intensity value compared to the background signal, which corresponded to Rose Bengal free in the solution. This analysis yields $GB \approx 13$ for a thickness of ~ 8 nm, and $GB \approx 7$ for a thickness of ~ 18 nm. These GB values correspond to the sum of the contribution of all molecules at distance greater than 8 or 18 nm, respectively. These values correlate with the predicted trend and can be taken as practical values. They are quantitatively in agreement with values reported recently.^{4e} Therefore, we can establish that the maximum enhancement in this simplified system with randomly oriented, low ϕ^0 fluorophores, is reached below 18 nm. Furthermore, there is a 2-fold increase in GB between 18 and 8 nm.

In identical experiments, performed with a Rhodamine B solution (Figure 5C), no significant contrast in the images acquired with the AuNPs of different SiO₂ shell thickness or with the SiO₂ NPs control sample (only images for 8 nm SiO₂ shell thickness are displayed). Particularly, no enhancement was observed for a shell thickness of 8 nm, the distance for which a maximum contrast was obtained when using Rose Bengal as fluorescent probe (Figure 5C). The fluorescence intensity was higher than that of Rose Bengal, and it was homogeneously distributed throughout the entire image, which made the AuNPs only detectable in the transmission channel.

Extending the Imaging Time Window of Fluorophores through Enhanced Photostability. The theoretical analysis presented above also suggests that a fluorophore in the vicinity of AuNPs exhibits an increased resistance to photodamage. This effect is of relevance to the field of Cell Biology since it could provide the means to selectively image fluorophores nearby a AuNP. Therefore, an increase in photostability would allow the study of processes with higher spatial and temporal resolutions. To prove the basis of a possible application, we performed experiments based on the interaction of fluorophores localized on actin filaments and endocytosed AuNPs (Figure 6).

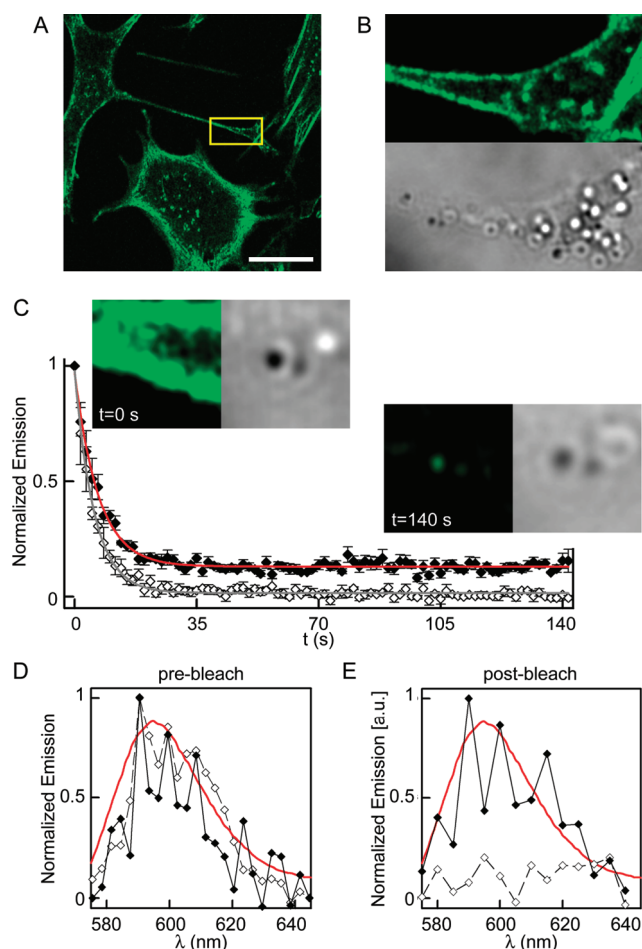


Figure 6. (A) Fluorescence imaging of actin filaments in fixed melanophore cells stained with Texas Red X-phalloidin. Scale bar: 20 μm . (B) Detailed view (from yellow rectangle in panel A) showing the fluorescence (top) and transmission (bottom) image. The AuNPs are clearly appreciated in the transmission image. (C) Normalized fluorescence bleaching curves performed on circular regions in the confocal image (diameter, 5 pixels) where the AuNPs colocalized with actin filaments (●) and on regions with actin filaments alone (○). The data correspond to means \pm standard error (s.e.) (sample set $n = 5$). The red and gray curves correspond to monoexponential fits to the data. A couple of fluorescence and transmission images from the same image portion are shown at the beginning of the bleaching irradiation ($t = 0$ s) and at the end of the experiment ($t = 140$ s). (D) Normalized pre- and (E) postbleaching emission spectra of Texas Red X-phalloidin acquired in regions with colocalized AuNPs and actin filaments (●) and in regions with actin filaments alone (○). Red curve: emission spectrum of a dilute solution of the fluorophore acquired in a fluorometer. The peak maxima of the pre- and postbleaching spectra of the fluorophore in close vicinity of the NP match that of the free dye.

The internalization of AuNPs by endocytosis has been reported in the literature²⁰ and constitutes a suitable experimental model for our purpose. Cells are able to uptake nanoparticles from their culture medium, and the resulting endosomes move along by interacting with cellular components such as actin filaments. Taking advantage of this process, we endocytosed AuNPs with $a = 30$ nm, fixed the cells, labeled the filaments with a fluorescent derivative of phalloidin (Figure 6A), and studied the response of the fluorophores in the vicinity of endocytosed AuNPs. (We did not use core-shell Au-SiO₂ NPs here because they were not stable in the culture medium and precipitated; it will be shown that the use of denuded AuNPs is

adequate as a proof of principle.) We selected Texas Red X phalloidin (TRedX-phal) as it displays the lowest ϕ^0 among commercially available labels ($\phi^0 \approx 0.5$),²¹ and thus, it is expected to provide the best contrast. The internalization of the nanoparticles was confirmed by acquiring the transmission images at the corresponding confocal microscope channel, exploiting the spectral features of the Au plasmon already characterized *in vitro*.

An examination of the fluorescence image after TRedX-phal labeling and the associated transmission image revealed the colocalization of some AuNPs and filaments (Figure 6B), in agreement with what was expected from the NP endocytic pathway. The fluorescence intensity along the filament was uniform in regions close and far away from the NP, a fact attributable to the relative high intrinsic ϕ^0 of the label. Therefore, we performed bleaching experiments to evaluate the persistence of the fluorophore and the emission spectral features as a function of the distance to the AuNP. From the photobleaching image sequences, we constructed normalized bleaching curves by selecting circular regions of interest (ROIs ~ 1 μm in diameter, in the order of $2\times$ the lateral confocal resolution) that were either associated to regions without AuNPs or to regions where actin filaments and AuNPs were colocalized (Figure 6C). The corresponding pre- and postbleaching emission and transmission images were also recorded.

The fluorescence of the TRedX rapidly faded and the fluorescence signal decreased to background levels in most of the image, a fact reflected in the bleaching curve obtained from all the tested ROIs that were not colocalized with AuNPs. In contrast, the bleaching rate for the fluorophore molecules colocalizing AuNPs was significantly delayed, and $\sim 15\%$ of the initial intensity value remained at long imaging times (i.e., minutes).

A quantitative analysis of both photobleaching time-decay curves revealed that they fitted well to a monoexponential law, with first order rate constants of 0.180 ± 0.004 s⁻¹ for the dye alone and 0.140 ± 0.004 s⁻¹ for dye molecules interacting with AuNPs. This represents a 20% increase in the characteristic bleaching time of TRedX due to the photoprotective effect exerted by a neighbor nanoparticle. We demonstrate that the remaining dye after complete photobleaching of background allows the effective imaging time to be increased from 20 s (what was needed for background bleaching) to more than 140 s, yielding a $7\times$ increase in the imaging time (Figure 6C).

To confirm that the emission signal corresponds to TRedX, we generated the pre- and postbleaching emission spectra on a pixel-by-pixel basis on the actin filament, far from a NP and on the NP, and compared them to the emission spectrum of a solution of the fluorophore (Figure 6E,F). In both cases, the spectra match that expected for TRedX, and no contribution from scattered light is observed.

Summarizing the previous observations and considering that Texas Red-phalloidin has $\phi \approx 0.5$, no fluorescence enhancement can be practically measured for this later dye, as Figure 6A,B,C shows. The contrast observed in Figure 6D appears as a result of the selective resistance to photobleaching of molecules in the vicinity of AuNP.

CONCLUSIONS

We investigated a series of parameters, NP radius (a), NP-F distance (h), F quantum yield, and F absorption and emission spectra, which are critical to understand the photophysical behavior of a fluorophore interacting with a metallic NP.

The analysis gives a global approach to this issue providing answers to key questions for the design of probes based on NP–F assemblies. In this regard, a critical point is the optimum NP–F distance to maximize GB. Our results show that the value for h depends mainly on ϕ^0 (Figures 1 and 2). From these calculations, it is possible to generate design plots that describe the optimum h for a NP–F system. In turn, the value for h to achieve the optimum GP (Figure 4) shows that extremely long imaging times with low brightness fluorophores can be achieved for $h \ll a$. In this case, once the distance, ϕ^0 , and emission wavelength of the fluorophore are known, GB can be estimated from Figures 1 and 3. A key point is determining the optimum ϕ^0 of the isolated fluorophore to achieve the better contrast between bound and unbound fluorophores. The theory predicts that this enhancement grows steadily with the decrease of ϕ^0 . The practical limit is dictated by a compromise between this increasing contrast and the decrease in the value of the product between the maximum GB and ϕ^0 , which gives the maximum brightness. Because of these opposite effects, the maximum brightness decreases much slower than ϕ^0 (Figure 2).

Another fundamental point reported here is that the fwhm for the enhanced region is reduced as ϕ^0 decreases. This relationship indicates how to choose a fluorophore suitable for optimizing the spatial resolution, thus allowing the observation of dynamics in a volume below the diffraction limit. Finally, because GP depends on the shape and the material of the NP whereas γ_{abs} depends only on the material properties, it is possible to separate the radiative term from the dissipative term by changing the geometry of the metallic NP and then increase GB even more.^{4b}

We provide experimental evidence for both aspects of fluorescence enhancement, namely, intensity and photostability. The capability of recording fluorescence from very low quantum yield molecules opens the promising possibility of detecting intrinsic fluorescence from species of relevance in biological systems, which are generally considered to be nonfluorescent. In turn, the capability of getting more photons from a molecule before photobleaching is demonstrated, which is useful in experiments requiring imaging over long periods of time. The increase in imaging time observed under the assayed conditions can be explained as the consequence of the increase in GP in the neighborhood of the AuNP. The fluorophores in the vicinity of the NP are more photostable, as predicted, and the spectral profile confirms that the remaining signal is due to fluorophores resisting photobleaching.

The theoretical approach presented here can be advantageously applied in the design of hybrid systems AuNP–F where the dyes are covalently attached to the metallic surface at optimum distances. Such hybrids would be of low toxicity²² and suitable for live-cell fluorescence microscopies with reduced background and long imaging times.

AUTHOR INFORMATION

Corresponding Author

*E-mail: pedro@qi.fcen.uba.ar.

Present Address

^{||}Laboratory for Fluorescence Dynamics, Department of Biomedical Engineering, University of California, Irvine, California 92697, United States.

ACKNOWLEDGMENTS

O.E.M., V.L., and P.F.A. are Research Staff from CONICET. L.C.E. thanks CONICET for a doctoral fellow. S.S. is a doctoral fellow and M.J.R. is a postdoctoral fellow from CONICET. This work was performed under financial support from ANPCYT (grant PICT 34193), UBA (grant X006), and CONICET (grant PIP 5470).

REFERENCES

- (1) (a) Thomas, K. G.; Kamat, P. V. *J. Am. Chem. Soc.* **2000**, *122*, 2655–2656. (b) Thomas, K. G.; Kamat, P. V. *Acc. Chem. Res.* **2003**, *36*, 888–98. (c) Tam, F.; Goodrich, G. P.; Johnson, B. R.; Halas, N. J. *Nano Lett.* **2007**, *7*, 496–501. (d) Ghosh, S. K.; Pal, T. *Phys. Chem. Chem. Phys.* **2009**, *11*, 3831–44. (e) Shim, S. Y.; Lim, D. K.; Nam, J. M. *Nanomedicine* **2008**, *3*, 215–32. (f) Bunz, U. H.; Rotello, V. M. *Angew. Chem., Int. Ed.* **2010**, *49*, 3268–79. (g) Swierczewska, M.; Lee, S.; Chen, X. *Phys. Chem. Chem. Phys.* **2011**, *13*, 9929–41.
- (2) (a) Ruppini, R. *J. Chem. Phys.* **1982**, *76*, 1681–1684. (b) Muskens, O. L.; Giannini, V.; Sanchez-Gil, J. A.; Rivas, J. G. *Nano Lett.* **2007**, *7*, 2871–2875. (c) Lakowicz, J. R. *Anal. Biochem.* **2005**, *337*, 171–194. (d) Kuhn, S.; Hakanson, U.; Rogobete, L.; Sandoghdar, V. *Phys. Rev. Lett.* **2006**, *97*, 017402. (e) Schneider, G.; Decher, G.; Nerambourg, N.; Praho, R.; Werts, M. H. V.; Blanchard-Desce, M. *Nano Lett.* **2006**, *6*, 530–536.
- (3) (a) Chen, Y.; Munechika, K.; Ginger, D. S. *Nano Lett.* **2007**, *7*, 690–696. (b) Fu, Y.; Lakowicz, J. R. *J. Phys. Chem. B* **2006**, *110*, 22557–22562.
- (4) (a) Lakowicz, J. R.; Shen, Y. B.; D'Auria, S.; Malicka, J.; Fang, J. Y.; Gryczynski, Z.; Gryczynski, I. *Anal. Biochem.* **2002**, *301*, 261–277. (b) Rogobete, L.; Kaminski, F.; Agio, M.; Sandoghdar, V. *Opt. Lett.* **2007**, *32*, 1623–1625. (c) Dulkeith, E.; Ringler, M.; Klar, T. A.; Feldmann, J.; Javier, A. M.; Parak, W. J. *Nano Lett.* **2005**, *5*, 585–589. (d) Nakamura, T.; Hayashi, S. *Jpn. J. Appl. Phys.* **2005**, *44*, 6833–6837. (e) Kim, J.; Dantelle, G.; Revaux, A.; Berard, M.; Huignard, A.; Gacoin, T.; Boilot, J. P. *Langmuir* **2010**, *26*, 8842–8849.
- (5) Estrada, L. C.; Aramendia, P. F.; Martinez, O. E. *Opt. Express* **2008**, *16*, 20597–20602.
- (6) Niu, J. L.; Zhu, T.; Liu, Z. F. *Nanotechnology* **2007**, *18*, 325607.
- (7) Graf, C.; Vossen, D. L. J.; Imhof, A.; van Blaaderen, A. *Langmuir* **2003**, *19*, 6693–6700.
- (8) Stober, W.; Fink, A.; Bohn, E. *J. Colloid Interface Sci.* **1968**, *26*, 62–69.
- (9) Rogers, S. L.; Tint, I. S.; Fanapour, P. C.; Gelfand, V. I. *Proc. Natl. Acad. Sci. U.S.A.* **1997**, *94*, 3720–3725.
- (10) Bharadwaj, P.; Novotny, L. *Opt. Express* **2007**, *15*, 14266–14274.
- (11) Enderlein, J. *Appl. Phys. Lett.* **2002**, *80*, 315–317.
- (12) (a) Encina, E. R.; Coronado, E. A. *J. Phys. Chem. C* **2007**, *111*, 16796–16801. (b) Novotny, L.; Hecht, B. *Principles of Nano-Optics*; Cambridge University Press: Cambridge, U.K., 2006.
- (13) Scaffardi, L. B.; Tocho, J. O. *Nanotechnology* **2006**, *17*, 1309–1315.
- (14) Carminati, R.; Neito-Vesperinas, M.; Greffet, J. J. *J. Opt. Soc. Am.* **1998**, *15*, 706–712.
- (15) Johnson, P. B.; Christy, R. W. *Phys. Rev. B* **1972**, *6*, 4370–4379.
- (16) Anger, P.; Bharadwaj, P.; Novotny, L. *Phys. Rev. Lett.* **2006**, *96*, 113002/1–4.
- (17) Fleming, G. R.; Knight, A. W. E.; Morris, J. M.; Morrison, R. J. S.; Robinson, G. W. *J. Am. Chem. Soc.* **1977**, *99*, 4306–4311.
- (18) Magde, D.; Rojas, G. E.; Seybold, P. G. *Photochem. Photobiol.* **1999**, *70*, 737–744.
- (19) Estrada, L. C.; Gratton, E. *Nano Lett.* **2011**, *11*, 4656–4660.
- (20) Chithrani, B. D.; Ghazani, A. A.; Chan, W. C. W. *Nano Lett.* **2006**, *6*, 662–668.
- (21) Lefevre, C.; Kang, H. C.; Haugland, R. P.; Malekzadeh, N.; Arttamangkul, S. *Bioconjugate Chem.* **1996**, *7*, 482–489.
- (22) (a) Badwaik, V. D.; Bartonjo, J. J.; Evans, J. W.; Sahi, S. V.; Willis, C. B.; Dakshinamurthy, R. *Langmuir* **2011**, *27*, 5549–5554. (b) Boisselier, E.; Astruc, D. *Chem. Soc. Rev.* **2009**, *38*, 1759–1782.